Desalination 592 (2024) 118161

Contents lists available at ScienceDirect

Desalination

journal homepage: www.elsevier.com/locate/desal

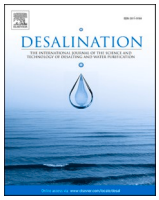

Cation selectivity during flow electrode capacitive deionization

Panyu Ren [a,b], Bin Wang [a], Jean Gustavo de Andrade Ruthes [a,b], Mohammad Torkamanzadeh [a], Volker Presser [a,b,c,*]

[a] INM - Leibniz Institute for New Materials, Campus D2 2, 66123 Saarbrücken, Germany
[b] Department of Materials Science & Engineering, Saarland University, Campus D2 2, 66123 Saarbrücken, Germany
[c] saarene - Saarland Center for Energy Materials and Sustainability, Campus C4 2, 66123 Saarbrücken, Germany

HIGHLIGHTS

- FCDI enables ion removal via continuous operation.
- Higher charge-to-size ratio favors bivalent cations in ion removal.
- Activated carbon content at 10 % mass optimizes FCDI performance.
- Conductive carbon black enhances ion uptake and separation efficiency.

GRAPHICAL ABSTRACT

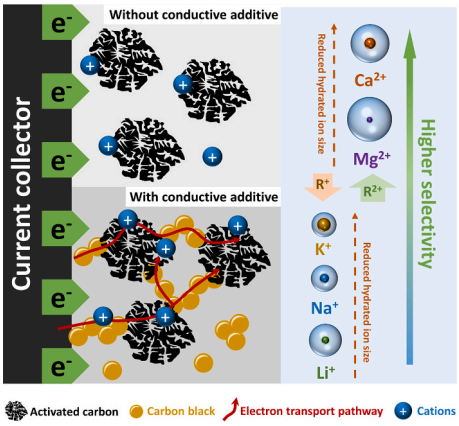

ARTICLE INFO

Keywords:
Activated carbon
Cation separation
Flowable electrode capacitive deionization

ABSTRACT

Efficient separation of specific ions from aqueous media is crucial for advanced water treatment and resource recovery. Flow electrode capacitive deionization (FCDI) offers potential for selective ion removal through continuous operation. This study evaluates the performance of selective cation separation using a commercial activated carbon slurry in a multi-ion solution of monovalent (Li^+, Na^+, K^+) and bivalent (Ca^{2+}, Mg^{2+}) cations. We assess ion removal and cation selectivity under different operational parameters, such as applied potential, slurry flow rate, and feed water flow rate. Our data show that bivalent cations, namely Ca^{2+} and Mg^{2+}, are preferentially removal due to their higher charge-to-size ratio, aligning with hydrated ion sizes. The highest separation rate was observed for Ca^{2+} (5.7 μg cm^{-2} min^{-1}), and the lowest for Li^+ (0.2 μg cm^{-2} min^{-1}). At the highest applied voltage (1.2 V), charge efficiencies reached 70 %, with an energy consumption of 41 Wh mol^{-1} for nearly complete cation removal. Optimal conditions were identified with a slurry flow rate of 6 mL min^{-1}, feed water flow rate of 2 mL min^{-1}, activated carbon content of 10 mass%, 1 mass% carbon black, and a cell voltage of 1.2 V. These findings highlight the importance of optimizing operational parameters to enhance ion removal.

* Corresponding author at: INM - Leibniz Institute for New Materials, Campus D2 2, 66123 Saarbrücken, Germany.
E-mail address: volker.presser@leibniz-inm.de (V. Presser).

https://doi.org/10.1016/j.desal.2024.118161
Received 13 August 2024; Received in revised form 25 September 2024; Accepted 26 September 2024
Available online 28 September 2024

1. Introduction

The accessibility of freshwater is increasingly challenged by the intersecting pressures of climate variability, burgeoning populations, expanding industrialization, and escalating contamination of water sources. [1] Commonly, water contains multi-salts like Li^+, Na^+, K^+, [2,3] hardness ions like Ca^{2+}, Mg^{2+}, [2,4] and toxic metal ions like Pb^{2+} and Cd^{2+} [5,6]. Toxic metal ions removal is important owing to their negative health and environmental impact, [7] while extracting precious elements, especially lithium, is strongly motivated by commercial interests in the wake of global electrification and rapid growth of battery production. [8] Hardness ions are also important for selective extraction due to scale formation in various applications employing hardness-ion-containing aqueous media, including, depending on the regional composition of the water, household devices like washing machines or dishwashers. [4]

Present-day water treatment methods mainly include technologies such as reverse osmosis (RO) [9] and thermal desalination methods such as multi-stage flash (MSF) [10] and multiple effect distillation (MED). [11] However, with a transition toward carbon neutrality and reduction of energy consumption, alternative water remediation and ion separation technologies with higher overall efficiency, lower energy consumption, and added functionality toward ion selectivity are intensively explored. [12,13] As one of these technologies, capacitive deionization (CDI) [14] is an electrochemical ion adsorption method used for the separation of salts, [15,16] toxic metal ions, [17,18] hardness ions, [19,20] and various anions [21] from water.

CDI typically uses static film electrodes, comprising either a layer of electrode material cast onto the current collector by a binder or a free-standing electrode placed in contact with the current collector. The performance (per cycle) is mainly determined by the salt adsorption capacity of the electrodes, which are charged and discharged cyclically. [22] The change from static film electrodes to suspended carbon particles in the flow electrode transitions CDI from cyclic charge/discharge (ion removal/ion release) operation toward continuous desalination. [23,24] The continuous operation also aligns more closely with the scalability requirements of electrochemical desalination in industrial settings, as it enables a steady process flow, ensuring consistent effluent water quality. [25] Another significant advantage of flow electrode CDI (FCDI) over CDI is the separate control over the system's capacity for ion removal and its rate of ion removal, analogous to the decoupled energy-power advantage of flow batteries. [26] That is, the desalination capacity in FCDI is determined by the volume of the flowable electrode (slurry tank), whereas the ion separation rate depends on the cell size (area of the membranes).

Over time, various FCDI cell and system configurations have emerged, including one-cell and two-cell setups, modifications of the current collectors, and an array of flow channel designs. [27–33] With its different technological variants, CDI offers unique benefits, including the capacity for precise or preferential removal of specific ions. [22,34] Selective ion removal is crucial because it can potentially recover specific valuable ions from water as a resource and target the specific removal of harmful species. [35] Various optimized materials and strategies have been developed for CDI to achieve selective ion separation. [36,37] Activated carbon (AC) enables selective ion separation by sieving specific ions based on the pore size. [38] For instance, Uwayid et al. demonstrated perfect selectivity for bivalent cations (Ca^{2+}) while excluding the competing monovalent Na^+ ions through an electrode made of sulfonated AC. [39] Subnanometer porous carbon developed by Zhang et al. achieved Cs^+ and K^+ selectivity factors of 3–4 compared to Na^+. [16]

Beyond nanoporous carbons, other electrode materials have been explored. [40] For example, copper hexacyanoferrate (Prussian blue analog) can selectively extract calcium ions. Xu et al. showed that charging the cell from 0.4 V to 1.2 V removes 127 μmol g^{-1} of bivalent Ca^{2+} while slightly expelling monovalent Na^+ in feed water containing 15 mM NaCl and 3 mM $CaCl_2$. [41] Demonstrated experimentally and by modeling, vanadium hexacyanoferrate prefers bivalent Ca^{2+} ions over monovalent Na^+ with a separation factor of $\beta_{Ca/Na} \approx 3.5$. [42] Additionally, multiple factors, such as ionic properties and operational parameters, affect the electrochemical ion-selective separation. Gao et al. observed preferential adsorption of multivalent cations from aqueous solutions with the order $Fe^{3+} > Cu^{2+} > Zn^{2+} > Na^+$, attributed to larger charge cations being more readily adsorbed onto electrode surfaces due to the electric field. [43] Among cations with the same valency, those with smaller hydrated radii were more effectively captured, as evidenced by $Cu^{2+} > Zn^{2+}$. [43]

While the research on ion selectivity has mainly focused on static electrodes, works have also started to explore ion selectivity for FCDI. For example, Zhang et al. employed FCDI to selectively separate Cu^{2+} in the coexistence of competing Na^+ from a saline solution with the assistance of electrodeposition in the short-circuited closed-cycle (SCC) mode. [44] Another study investigated the selective phosphorous recovery through the adjustment of charging and discharging procedures of the FCDI system, [45] which achieved a satisfactory phosphorus recovery performance (164 mg L^{-1} at each cycle) and selectivity factors above 2 (versus Cl^-) under optimized conditions (i.e., a carbon content of 5 mass%, charge and discharge current densities of +10 A m^{-2} and -15 A m^{-2}, respectively). Other strategies to induce selectivity in FCDI systems include functionalizing the ion-exchange membranes, where a favorable sodium extraction from Na^+/Ca^{2+} mixtures has been reported. [46]

Unlike the abundant research on mono−/multivalent cation-selective separation via CDI, selective ion separation via FCDI remains underexplored in the scientific community. This work systematically investigates the selective cation removal performance of AC and other carbon materials in multi-salt (Li^+, Na^+, K^+, Ca^{2+}, Mg^{2+}) mixed solutions under different operational parameters. We investigated the selectivity of AC toward cations (Na^+, K^+, Ca^{2+}, Mg^{2+}) compared to Li^+ as a function of the AC content, cell voltage, flow rate, and the mass loading of carbon black introduced as a conductive additive.

2. Materials and methods

2.1. Materials

Commercially available activated carbons (ACs) of YP-80F (AC1, Kuraray Chemicals Co.), YP-50F (AC2, Kuraray Chemicals Co.), and MSP-20 (AC3, Kansai Coke and Chemicals) were used. To serve as a conductive additive, we used VULCAN XC72R Specialty carbon black (CB, CAS No. 1333-86-4) from Cabot. Lithium chloride (LiCl, CAS: 7447-41-8, 99 %), sodium chloride (NaCl, CAS: 7647-14-5, 99 %), potassium chloride (KCl, CAS: 7447-40-7, 99 %), magnesium chloride ($MgCl_2$, CAS: 7786-30-3, 99 %), and calcium chloride ($CaCl_2$, CAS 10043-52-4, 99 %) were purchased from Sigma Aldrich. Cation and anion exchange membranes (Fumasep FKS-PET-130/ED-100 and Fumasep FAS-PET-130/ED-100, Fumatech) were employed in the FCDI cells. Deionized water (resistivity: 18 MΩ cm^{-2}) obtained from a Mili-Q purification system was utilized throughout this research.

2.2. Material characterization

Scanning electron microscopy (SEM) was performed using a ZEISS GEMINI 500 with an accelerating voltage of 1 kV for imaging. The electrode materials were attached to an adhesive Cu foil on the Al sample holder without additional sputter-coating. Nitrogen gas sorption analysis (GSA) was conducted by an iQ system (Quantachrome; formerly Anton-Paar) at −196 °C. The samples were first degassed at +300 °C for 24 h to remove humidity. The specific surface area (SSA) was calculated using the ASiQwin software following the Brunauer-Emmett-Teller (BET) equation.

The viscosity of slurries was examined through rheological studies

using an Anton Paar MCR 302e rheometer equipped with a stainless-steel concentric cylinder cup geometry to minimize particle settling. Measurements were conducted at shear rates ranging from 0.001 s^{-1} to 200 s^{-1}, maintaining a constant temperature of 25 °C throughout all experiments. The experimental data was evaluated with the Ostwald-de Waele power-law model presented in Eq. (1):

$$\eta = k \bullet \gamma^{n-1} \quad (1)$$

where η is the viscosity, k is the consistency index, and n is the shear thinning index. The data analysis is reported in Table 1.

2.3. FCDI cell operation and performance calculations

10 mass% AC and 1 mass% CB were soaked in the solution, which contained the same composition as the feed water. The mixture was sonicated for 1 h and stirred for another 3 h before pumping into the cell. The slurry was continuously stirred on a magnetic stirrer during the experiment to maintain homogeneity and avoid precipitation. The schematic diagram in Fig. 1 displays the experimental setup of our FCDI system utilizing single cycle (SC) mode. [47] A single cell operates with the feed water channel between the cation and anion exchange membranes and flowable electrode channels on either side of the ion exchange membranes. The FCDI cell is powered using an electrochemical potentiostat (VSP300, Bio-Logic). The feed electrodes (FE, carbon slurry) stored in the reservoir are pumped through the flow electrode channels. As they flow out of the flow channels, they are returned to the reservoir and constantly recirculated, forming the SC mode in which the anions and cations can neutralize in the reservoir. The bottom panel of Fig. 1 shows the flow channel cut according to the cell structure using the rubber sheet with ~4 mm width.

Previous studies have investigated the effect of initial feedwater salt concentration on FCDI performance, demonstrating its significant impact on desalination efficiency and energy consumption. [48,49] Our multi-component salt solution contained 10 mM Li^+, 10 mM Na^+, 10 mM K^+, 10 mM Ca^{2+}, and 10 mM Mg^{2+}, used as both the feed water channel and the supporting electrolyte of the slurry to maintain the same concentration across those channels, to minimize ionic migration due to unequal osmotic pressure. The latter solution was also used to soak all ion exchange membranes overnight. To investigate the effect of the flow rates on the cation separation performance, the flow rates of feed water were set as 1 mL min^{-1}, 2 mL min^{-1}, and 4 mL min^{-1}, while the flow rate of electrodes slurry was set at 6 mL min^{-1}, 12 mL min^{-1}, and 24 mL min^{-1}.

Inductively coupled plasma optical emission spectroscopy (ICP-OES) was used to quantify the cation separation in a mixed cation system. Samples were extracted from the feed water reservoir of the FCDI system at time intervals of 0 h, 4 h, 8 h, 12 h, 24 h, and 32 h, diluted with Mili-Q water and tested by ICP-OES offline mode. This ICP-OES mode can be flexible in sample collection and processing and can analyze samples in batch mode rather than quasi-real-time. ICP-OES tests were repeated three times for each sample, with the mean value used for analysis. Before the offline test, we constructed the relationship between each ion concentration and the correspondent ICP signal intensity following the procedure outlined in our previous work. [50] Briefly, mixed ion solutions with known concentrations of 0.2 mM, 0.5 mM, 1 mM, 2 mM, 5 mM, and 10 mM LiCl, NaCl, KCl, $CaCl_2$, and $MgCl_2$ were used for the calibration.

Table 1
Rheological parameters of the activated carbon suspension electrodes.

Carbon content	Carbon black content	Consistency index (k)	Shear thinning index (n)
10 mass% AC1	1 mass%	0.41	0.59
10 mass% AC2	1 mass%	0.25	0.41
10 mass% AC3	1 mass%	0.24	0.35
10 mass% AC1	0 mass%	0.38	0.40
10 mass% AC1	2 mass%	0.592	0.56
5 mass% AC1	1 mass%	0.22	0.46
15 mass% AC1	1 mass%	0.78	0.68

The performance metrics of FCDI cells were analyzed regarding ion separation ratio (ISR), average ion separation rate (AISR, μg cm^{-2} min^{-1}), ion selectivity factor (ISF), charge efficiency (CE, %), and average energy consumption (AEC, Wh mol^{-1}). ISR is defined as the concentration ratio of a specific cation in the treated water to initial feed water by following Eq. (2):

$$ISR = \frac{C_t}{C_0} \quad (2)$$

where C_t is the ion concentration (mM) at time t, and C_0 is the initial ion concentration (mM). As such, an ISR value of unity for a specific ion indicates the system's indifference toward that ion, whereas an ISR value close to zero means a complete removal of that ion from the feed by the system.

AISR is measured to assess the salt removal rate per unit geometric contact area between target water and electrode slurry, which is calculated following Eq. (3):

$$AISR = \frac{(C_0 - C_t) \times V}{S_A \times t} \quad (3)$$

where V is the volume of feed water (mL), S_A represents the effective contact area (cm^2), and t is the operation time of the FCDI system.

ISF_i is defined as the ion selectivity of the FCDI system toward a specific ion compared to Li^+, which is obtained using Eq. (4):

$$ISF_i = \frac{\Delta C_i}{\Delta C_{Li^+}} \quad (4)$$

where ΔC_i represents the concentration change of a specific cation in the outflow reservoir (mol L^{-1}), and ΔC_{Li+} is the molecular concentration change of lithium in the outflow reservoir (mol L^{-1}).

CE is defined as the ratio of ionic charge (salt) removed to the invested electric charge (electrons) calculated using Eq. (5):

$$CE = \frac{\sum \Delta C_f \times z \times V \times F}{(\int I\, dt)} \times 100\% \quad (5)$$

where F represents the Faraday constant (96,485 C mol^{-1}), z is the valency (e.g., z = 1 for Na^+ and z = 2 for Mg^{2+}), $\sum \Delta C_f$ is the sum of concentration changes (mM) of all ionic species in the process, I is the real-time current monitored by the electrochemical workstation, and dt is the duration during which the latter current and concentration changes were measured.

AEC (Wh mol^{-1}) is defined as the invested energy to remove one mole of salt. The latter could be expressed as the product of applied cell voltage E (V) and the measured charge divided by the number of moles of salt removed by the FCDI system, *V* is the volume of the feed water (L). following Eq. (6):

$$AEC = \frac{(\int I\, dt) \times E}{(C - C_0) \times V} \quad (6)$$

3. Results and discussion

3.1. Cation separation performance of different carbon materials

Three commercial carbon materials with different pore characteristics and surface features, AC1, AC2, and AC3, were used as flowable carbon electrodes for our FCDI system (Fig. 2). Nitrogen sorption isotherms provided the total pore volume of AC1, AC2, and AC3 as 1.4 cm^3 g^{-1}, 0.84 cm^3 g^{-1} and 0.94 cm^3 g^{-1}, with the mean pore size of 1.6 nm, 0.76 nm, and 0.81 nm, respectively (*Supporting Information,* Table S1). The size and shape of the AC particles differed for the different

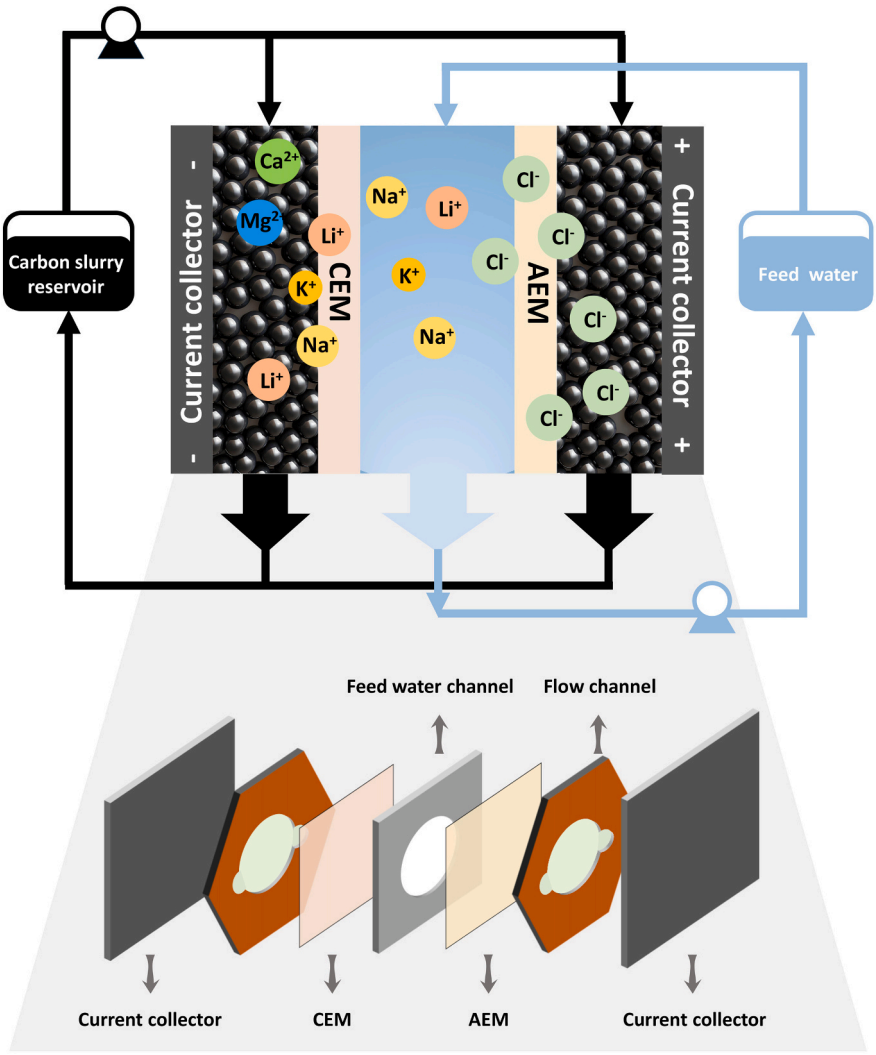

Fig. 1. Schematic illustration of the cell structure of flowable electrode capacitive deionization system, the experimental setup, and the operating principle.

materials. AC1 and AC2 are very similar (*Supporting Information*, Fig. S1A–D), consisting mainly of large, coarse particles tens of micrometers wide and numerous smaller particles. In contrast, AC3 has a relatively large particle compared to those surrounded by debris (*Supporting Information*, Fig. S1F). Scanning electron micrographs of the conductive carbon black additives sample show a finer and smaller particle size (*Supporting Information*, Fig. S1G–H).

A decreasing concentration trend was observed for the three carbons, gradually separating most of the monovalent and multivalent cations from the bulk solution throughout 32 h (Fig. 2A–C). The FCDI system followed the ion removal order of $Ca^{2+} > Mg^{2+} > K^{+} > Na^{+} > Li^{+}$. This order relates to the varied valence and hydration radius of these ions. [16] That is, the ions with higher valency are more effectively removed via ion electrosorption in equilibrium, which is in agreement with the order of the adsorption rate consistently observed in our FCDI system: Ca^{2+} and Mg^{2+} removal exceeded that of K^{+}, Na^{+}, and Li^{+}. [51,52] Three carbon materials also showed different cation separation rates and efficiency due to varied porous features. AC1 showed the fastest cation separation and highest ion removal efficiency, almost completely removing all ionic species after 32 h. Also, AC1 removed nearly 60 % of Li^{+} and 100 % of Ca^{2+} from the solution within 24 h, whereas the Li^{+} removal was 24 % for AC2 (Ca^{2+}: 88 %) and 39 % for AC3 (Ca^{2+}: 86 %) after the same time. Accordingly, the calculated average cation separation rates for AC1 were noticeably higher than the other two carbons, as illustrated in Fig. 2D–F.

When operating the systems for 12 h, the average separation rate of Ca^{2+} (5.7 μg cm^{-2} min^{-1}), Mg^{2+} (2.8 μg cm^{-2} min^{-1}), K^{+} (3.3 μg cm^{-2} min^{-1}), Na^{+} (0.9 μg cm^{-2} min^{-1}) and Li^{+} (0.2 μg cm^{-2} min^{-1}) was shown by AC1 flowable electrode. Within the same duration, AC2 and AC3 showed lower average separation rates. The superior performance of AC1 could be ascribed to its higher pore volume and broader pore size distribution compared to AC2 and AC3 (*Supporting Information*, Fig. S2B). Initially, the removal rate of bivalent cations (Ca^{2+} and Mg^{2+}) for all three carbon electrodes was generally much higher than that of monovalent cations (K^{+}, Na^{+}, and Li^{+}). Then, it decreased with prolonged operation time while more monovalent cations began to be captured. The separation sequence of ions was determined by their valance and hydration radius. The higher charge/hydration size ratio of Ca^{2+} and Mg^{2+} ensured a more sensitive response to the electrical field, facilitating the uptake of these bivalent cations by flow electrode. Among the monovalent cations, K^{+} showed the highest separation rates, attributed to the highest ion mobility for K^{+} compared to Li^{+} and Na^{+}. [53] According to the results above, AC1 was selected for the subsequent optimizations of FCDI system performance.

The effect of the carbon additive was further evaluated with different AC carbons, as displayed in *Supporting Information,* Fig. S3. Although with slight deviations in the viscosity, attributed to the different particle size and arrangement of the aggregated structures, the impact of the different morphologies of each AC over the viscosity indicates a synergistic behavior between AC1 and CB, enabling a more packed flow

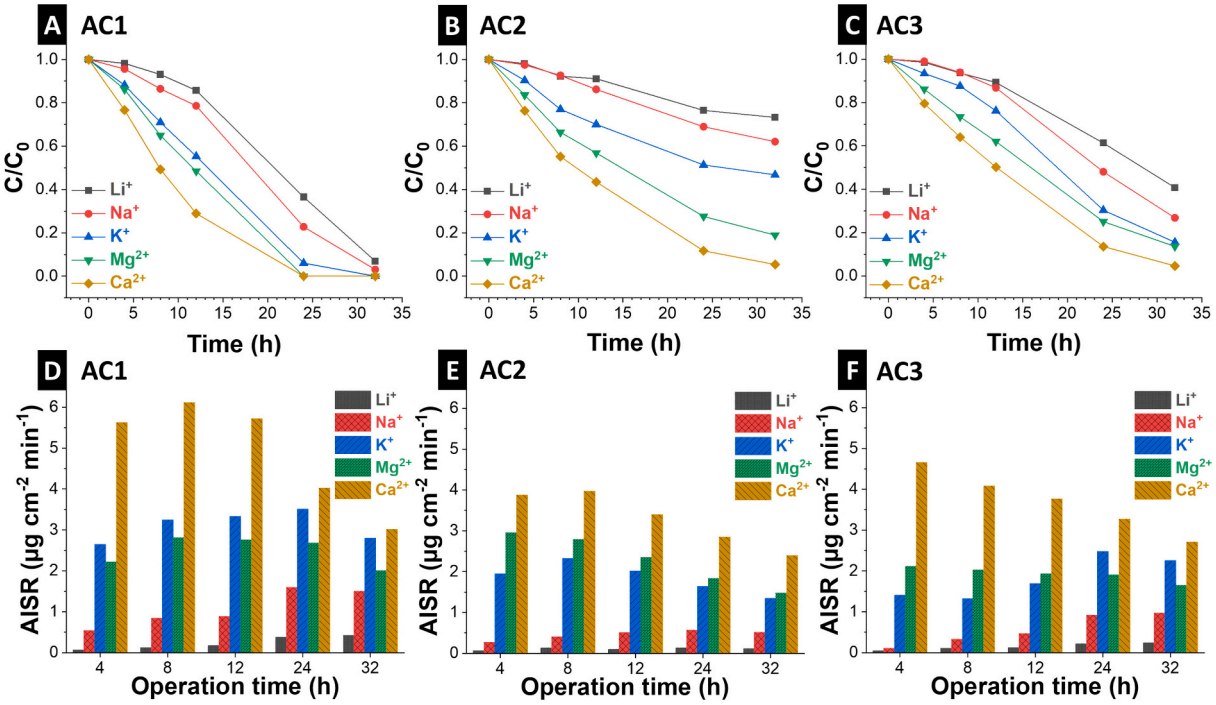

Fig. 2. Ion separation and average ion separation rate of different carbon materials: (A and D) AC1, (B and E) AC2, (C and F) AC3 at a flow rate of 6 mL min^{-1} for flowable electrode and 2 mL min^{-1} for feed water, with 10 mass% of carbon and 1 mass% CB at 1.2 V.

network with higher conductivity, consequently increasing the selectivity factor.

3.2. *Effect of conductive additives and AC mass content*

The FCDI setup, with its flow electrode particles dispersed in the electrolyte solution, inherently limits effective charge transfer between different electrode particles and the solid-liquid interface. Conductive additives such as carbon black are commonly used to increase electrical conductivity, as the added particles act as a conductive bridge between suspended AC particles and the current collector or between different suspended AC particles. [15,54] The carbon black additive is utilized in this study to enhance the performance of poorly conductive suspension electrodes in our FCDI systems. We studied how introducing carbon

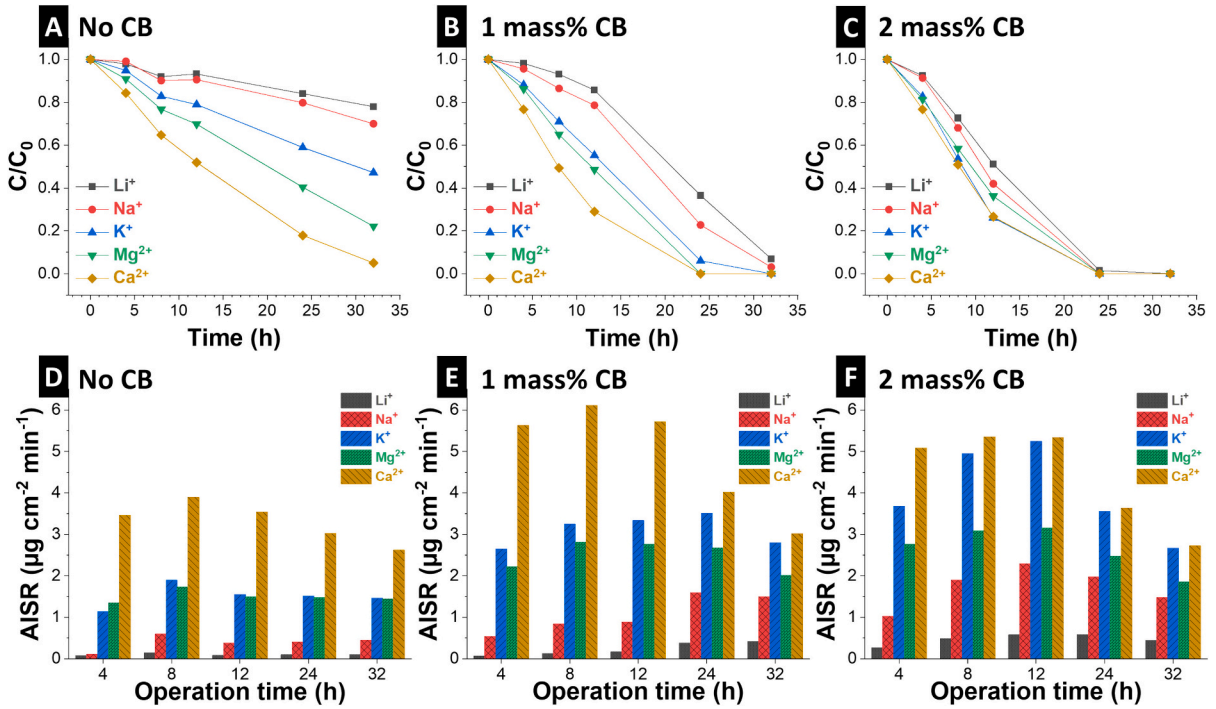

Fig. 3. Ion separation curve and average ion separation rate at different CB content: no carbon black (A, D), 1 mass% CB (B, E), and 2 mass% CB (C, F). For all data, the flow rate was 6 mL min^{-1} for the flowable electrode and 2 mL min^{-1} for the feed water, with a mass loading of 10 mass% AC1.

black as an additive affects the cation selectivity and/or removal rates. To this end, different amounts of carbon black (no addition, 1 mass%, and 2 mass%) were added to the carbon slurry to evaluate the effect of conductive additives on FCDI performance (Fig. 3).

The addition of CB notably facilitated the separation of ions, especially the monovalent cations (Li^+, Na^+, and K^+). This trend was further observed at a high CB content of 2 mass%. With the CB content increasing from 0 mass% to 2 mass%, the average Ca^{2+} separation rate increased from 3.5 μg cm^{-2} min^{-1} to 5.3 μg cm^{-2} min^{-1}, and there was a significant increase from 0.1 μg cm^{-2} min^{-1} to 0.6 μg cm^{-2} min^{-1} (~ 6 times higher than the blank) for Li^+. A similar trend was also observed for the separation profile of Na^+ and K^+, increasing the separation rate from 0.4 μg cm^{-2} min^{-1} and 1.6 μg cm^{-2} min^{-1} to 2.3 μg cm^{-2} min^{-1} and 5.2 μg cm^{-2} min^{-1}, respectively. Additionally, to study whether the CB alone as a conductive agent in the flow electrode can adsorb cations, we tested 1 mass% CB without any AC. As shown in the *Supporting Information*, Fig. S4, having other parameters constant, no significant reduction in ion concentration occurs when the AC is absent in the slurry solution.

Viscosity analysis of the AC1 sample with different CB content (Fig. 4A) demonstrated a shear-thinning, or pseudoplastic, behavior for all the electrodes, indicating a fluid structure with a finite yield stress with a viscosity of 64 mPa•s at a shear rate of 20 s^{-1}. [55,56] Upon adding carbon additive (carbon black), the viscosity increased at the same shear rate, achieving values of 180 mPa•s with 1 % CB and 268 mPa•s with 2 % CB. Simultaneously, the rheological behavior of the samples with the CB additive displayed a rise in the viscosity at 20 s^{-1}, which can be attributed to the agglomeration of carbon particles. [57]

The impact of CB addition is also noted in the selectivity of lithium ions, as presented in Fig. 4B–D. This can be attributed to the packing effect promoted by the different particle sizes of AC1 and CB (*Supporting Information*, Fig. S1A,H), which increased the connectivity and electric conductivity of the flow network while allowing the flow of aqueous media. [58–60] Furthermore, the additive particles increase interactions with the feed water and more friction between the carbon particles, promoting repulsion forces that lead to higher viscosity at low shear rates and facilitate the formation of agglomerates, as observed in 20 s^{-1}. [60–62] As the shear rate increases, the interactions between particles are less effective, hence the drop in viscosity values. [61–63] Besides CB additive effects, AC serves as the active mass content in the slurry that predominantly determines the cation separation performance of our FCDI system. The active electrode material allows charged ions to be captured and stored in its nanostructure by ion electrosorption. In addition, the AC content also dictates the viscosity of electrode slurry, particle density, and, thereby, the slurry channel's conductivity, which could significantly affect operation stability and efficiency. [64] As such, the effect of AC content in the slurry was studied at mass loadings of 5 %, 10 %, and 15 % (Fig. 5).

As observed in Fig. 5A–C, an enhanced ion removal was achieved at higher AC1 mass contents. While only 14 % of Li^+ and 67 % of Ca^{2+} were captured after 36 h operation at a mass loading of 5 %, nearly all the ions were removed at a mass loading of 10 %. Previous reports [4] linked this trend to the decreased charge and ion transfer owing to fewer available electrode sites and particle collision due to reduced viscosity and particle density of the electrode slurry. Although faster ion removals were obtained from 10 mass% to 15 mass% AC1, the latter composition resulted in a very dense slurry and the consequent particle aggregation and clogging issues (*Supporting Information*, Fig. S5) both in the flow

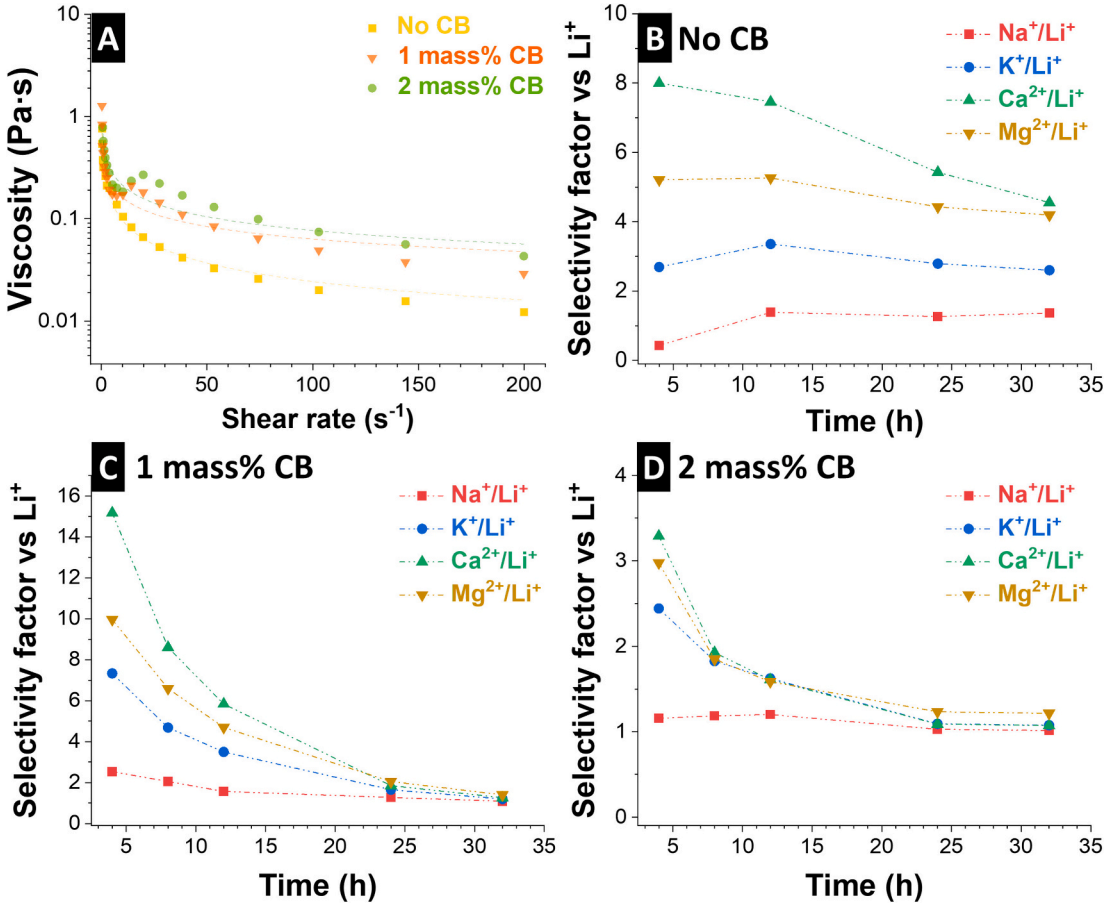

Fig. 4. (A) Rheological behavior of the flowable electrode at three CB contents; Ion selectivity factors at different CB contents of (B) 0 mass% CB, (C) 1 mass% CB, and (D) 2 mass% CB at a flow rate of 6 mL min^{-1} for flowable electrode and 2 mL min^{-1} for feed water, with 10 mass% of AC1 and different CB content at 1.2 V.

channel and tubes. As such, 10 % of the carbon mass was chosen as the highest content feasible for the efficient and stable operation of our FCDI system. So far, various approaches have been reported to address the limitation of flowability with high mass loading, e.g., by oxidizing the active material (increased repulsion between particles) to achieve less aggregation or by mixing two different particle sizes of activated carbon (broadening the particle size distribution) to improve the flowability of the slurry. [59] Additionally, surface-modified AC particles can be used as a dispersant for hydrophobic AC particles in aqueous solutions. [65,66] One can also modify the surface chemical properties of electrode particles to suppress the flow electrode clogging in an FCDI cell.

To better understand the role of the AC1 mass loading, viscosity analysis was performed on electrodes with different mass amounts and the absence of carbon additives (carbon black). The viscosity curves are presented in Fig. 5D, where the pseudoplastic behavior of the carbon electrodes is maintained, although with a broader range of agglomeration at small shear rate values due to the bigger particle sizes of AC1. [59,63] The consistency of slurries is also affected, as shown in Table 1, where the increase in the mass of AC1 with the rise in k (consistency) values indicates a more viscous material. [63,67]

We further investigated the merits of our FCDI system in terms of cation selectivity vs. Li^+ ions. Selectivity profiles (vs. Li^+) of the ions with different carbon black contents were calculated from the data presented in Fig. 3 and plotted in Fig. 4. Gradually reducing selectivity factors of Ca^{2+}, Mg^{2+}, K^+, and Na^+ with respect to Li^+ are observed within the investigated time intervals. Compared to Li^+, other cations were preferentially removed from the bulk solution within the first few hours, with the selectivity order related to the hydrated radius and valency of these cations (Fig. 6). When an electrostatic field is applied, cations (Ca^{2+} and Mg^{2+}) with higher valence charges undergo stronger electrostatic driving force compared to monovalent cation, which causes their faster electrokinetic behavior and migration from bulk solution to slurry channel. [68] Regarding cations with the same valance, ion selectivity will be mainly regulated by the hydrated radius of different cations, which is related to the resistance and mobility of these ions in solution. [69] According to the Stokes-Einstein relation, the self-diffusion coefficient of an ion in water is inversely proportional to its effective radius; [70] an ion with a smaller radius has higher mobility in aqueous solution. The higher mobility and transport kinetic also facilitate ion diffusion into the inner pore structure of carbon particles, causing preferable capture and storage within the pore volume. Bivalent cations Ca^{2+} have a smaller hydrated radius than bivalent Mg^{2+} (4.12 Å vs. 4.28 Å). As a result, Ca^{2+} shows higher transport ability and preferable selectivity compared to Mg^{2+}. Overall, monovalent cations exhibit lower removal rates and selectivity than divalent cations due to valence difference and follow the removal order of $K^+ > Na^+ > Li^+$, which agrees with their hydrated radius difference (*Supporting Information,* Table S2).

During continuous ion removal by flowing electrode, cations are generally adsorbed onto the flowable carbon particles with a negative

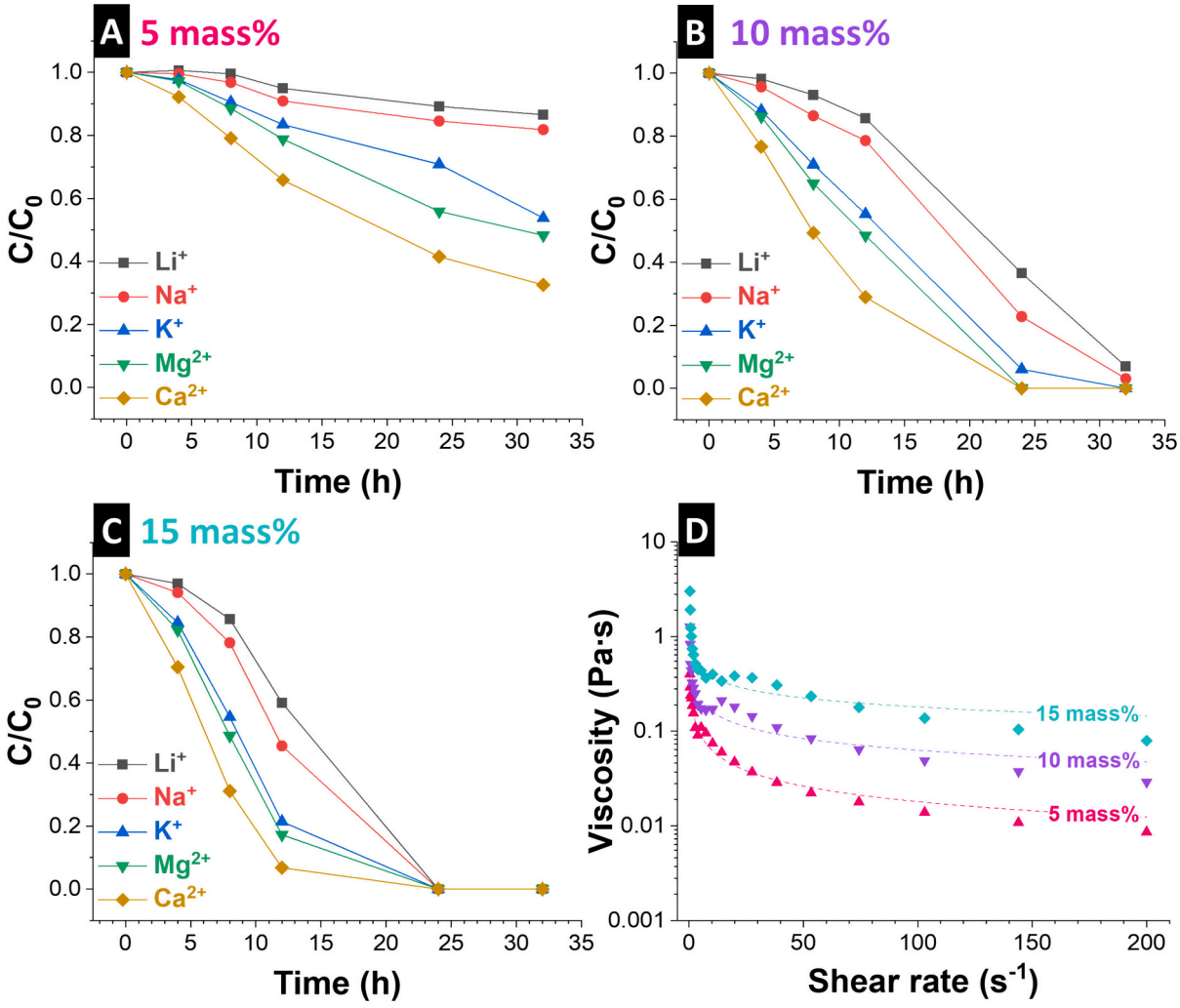

Fig. 5. Ion separation over time of different carbon content: (A) 5 mass%, (B) 10 mass%, and (C) 15 mass%, at a flow rate of 6 mL min^{-1} for flowable electrode and 2 mL min^{-1} for feed water, with 1 mass% CB at 1.2 V. (D) Rheological behavior of the flowable electrode at three AC1 contents (5 mass%, 10 mass%, 15 mass%).

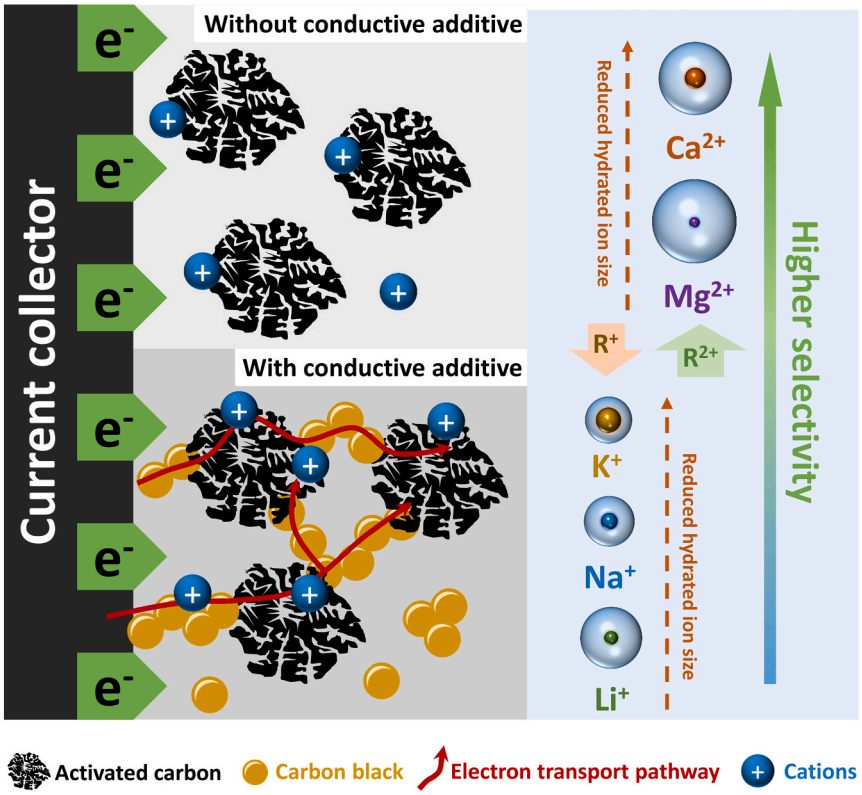

Fig. 6. Schematic illustration of ion separation and selectivity in the FCDI system with and without the addition of carbon black.

charge under the force of an electric field and then carried along with the carbon material into the slurry reservoir by pumping. Since our FCDI system uses the SC mode, these cations will eventually be neutralized by anions (Cl^-) in the slurry reservoir. Hence, bivalent cations are more readily adsorbed on the flowable electrode surface than monovalent cations, resulting in higher electrosorption selectivity as well Regulated by intrinsic hydrated radius and valency, the mobility and transport of investigated cations in aqueous solution vary under the driving force of the electrostatic field, rendering ion removal by flowable electrodes following the consequence of $Ca^{2+} > Mg^{2+} > K^+ > Na^+ > Li^+$. The specific selectivity also comes from the preferable capture and storage of divalent cation on electrode carbon nanopores to screen the negatively charged AC surface. Compared to Li^+, other cations will preferably be removed from the feed at the initial stage. Li^+ remains in the solution, while other cations can be taken up more quickly from the feed. Benefiting from higher residual concentration, Li^+ becomes more competitive, and the dynamic interaction between Li + and electrode surface increases, causing a gradual decrease in ion selectivity with time.

FCDI without carbon black additive, which had the slowest cation separation kinetics (Fig. 3A), exhibited modest selectivity factors of 1.0–5.0 for Ca^{2+}, Mg^{2+}, K^+, and Na^+ vs. Li^+ at the end of experiments. Although adding 1 % or 2 % mass carbon black could largely enhance ion removal kinetics, the cation selectivity factors decrease to below 2. Overall, adding CB could accelerate the migration and uptake of cations, especially monovalent cations Na^+ and Li^+, resulting in low selectivity factors of Ca^{2+}, Mg^{2+}, K^+, and Na^+ versus Li^+. As Li^+ ions possess significantly larger hydration sizes than hydrated Na^+ and K^+ ions, [71] the system exhibits a reduced selectivity toward the uptake of Li^+ ions and, hence, an overall preference for bivalent cations. In this case, conductive carbon black could act as a conductive bridge (Fig. 6) between electrode particles and charged ions and between different electrode particles, [47,72,73] enhancing charge transfer in the solid-electrolyte interface and facilitating electrochemical migration and storage of charged species on electrode materials (Fig. 6). Similarly, Reale et al. reported that the size and mass fraction of conductive additives could affect the effective electronic conductivity, ionic conductivity, and hydraulic permeability of porous electrodes, and increasing any one of these properties could increases salt removal rate at fixed specific energy consumption [74].

Considering ions separation performance, selectivity behavior, and mass loading amount, 1 mass% of carbon black was used in this study as a conductive additive content.

As illustrated by Fig. 2A–C, different types of AC show similar selectivity trends for monovalent and bivalent cations ($Ca^{2+} > Mg^{2+} > K^+ > Na^+ > Li^+$). However, AC1 has a relatively higher affinity toward monovalent cations than AC2, which prefers bivalent cations. The latter is attributed to a broader pore size distribution of AC1 (*Supporting Information*, Fig. S2B). With the same cation concentrations, cations with smaller hydrated radius, for example, K^+ (3.31 Å, *Supporting Information,* Table S2), show a higher selectivity than Li^+ (3.82 Å, *Supporting Information,* Table S2), exhibiting their size-affinity to access the pores in the flowable carbon particles. A similar observation is found for bivalent cations. For example, Ca^{2+} with a smaller hydrated ion size (4.12 Å, *Supporting Information,* Table S2) shows a higher cation selectivity than Mg^{2+} (4.28 Å).

3.3. *Effect of applied voltage*

During FCDI operation, the applied potential bias serves as the driving force that induces the migration of ions from the bulk solution toward the electrode surface. [75] This migration process significantly influences both desalination efficiency and adsorption capacity. In theory, higher voltages result in stronger electrostatic forces. However, the applied voltage in CDI is typically limited to below 1.2 V to prevent faradaic side reactions like water electrolysis when the voltage exceeds 1.23 V. [76] Furthermore, excessive electrostatic forces may cause high mobility of all ions, thereby reducing selectivity toward target ions. As such, the applied voltage is an influential operational parameter that

plays a crucial role in ion migration rates, influencing the overall cation separation performance.

The cation separation behavior of the FCDI system was studied with the applied voltages of 0.4 V, 0.8 V, and 1.2 V, as demonstrated by Fig. 7. Additionally, the applied cell voltage and the current response profiles of the latter 3 tested voltages can be found in *Supporting Information,* Fig. S6. As seen, the overall ion removal performance was very low at 0.4 V, with only 13–68 % of initial ions removed after 32 h operation. In contrast, cation separation (especially monovalent cations) was more effectively accomplished at 0.8 V and 1.2 V. Going from 0.4 V to 0.8 V, the Li^+, Na^+, and K^+ separation performance experienced a notable increase from 14 %, 21 %, and 40 % to 80 %, 84 %, and 98 %, respectively. The Ca^{2+} and Mg^{2+} ions could be entirely removed by the FCDI system already at 0.8 V. The cation separation was further enhanced at 1.2 V, with the removal efficiency of all ions over 93 %. The CE profile at different applied voltages was also enhanced from 63 % to 70 % when the cell voltage increased from 0.4 V to 1.2 V. The energy consumption increased slightly from 0.4 V to 1.2 V, with 40.6 Wh mol^{-1} required to remove all cations from the feed water at 1.2 V (Fig. 7D).

Energy consumption data and the average cation separation rate of the FCDI cell at different conditions were summarized in *Supporting Information,* Table S3. Compared to AC2 and AC3, AC1 could maintain the highest cation separation rate at the end of the experiment with the lowest energy consumption. Adding 1 mass% conductive CB could decrease systematic energy consumption from 49.2 Wh mol^{-1} to 40.6 Wh mol^{-1}, whereas more energy-intensive operation of FCDI was observed when CB content increased to 2 mass%. A similar trend was also observed in the mass loading range of 5–15 mass%, showing that the adjustment of operation parameters is of great significance in improving the energy efficiency of the FCDI system.

3.4. Initial techno-economic analysis

Understanding the economic viability of the FCDI system is crucial for real-world applications in water treatment and resource recovery. [77,78] The primary capital cost of the FCDI cell and infrastructure, including the modules, pumps, power supplies, and control systems, constitutes the major expense for a one-time setup of a pilot-scale system. [79,80] Once the latter is installed, the operational costs encompass material replenishment and energy consumption. The expenses for activated carbon vary greatly based on its quality, which in turn depends on the source of raw material used for its production and its pyrolysis and activation routes. As such, prices as low as ~1 € per kg have been reported for commercial-scale activated carbon production in Africa. [81] For supercapacitor-grade activated carbons, higher costs of 10–15 € per kg can be assumed. Taking a conservative estimate of 15 € per kg for the price of high-performance AC1, the cost for the 4 g used in the slurry solution would be 0.06 €. Since carbon black constituted only a minor part of the slurry solution, it has been neglected in our calculations.

The energy consumption includes the electrical energy invested to charge the system and the pumping energy. As outlined above, the charging energy required to remove cations from the feed solution within 32 h of operation at a cell voltage of 1.2 V is approximately 41 Wh mol^{-1}. Given the volume of feed solution at 80 mL and each salt concentration of 10 mM, this translates to total salt moles of 4 mmol. An energy consumption of 41 Wh mol^{-1} means 0.164 Wh of energy consumed per cycle to remove all the cations from the feed solution.

Given the 32 h of operation of the peristaltic pump with a maximum power of 15 W, the pumping energy is estimated at a maximum of 0.48 kWh. As the charging energy is negligible compared to the latter pumping energy, the overall electricity consumption depends on the pumping at 0.48 kWh per cycle. Assuming an average electricity price in Germany in the second half of 2023 (0.402 € per kWh, Eurostat 04/2024) for household consumers, the pumping energy consumption

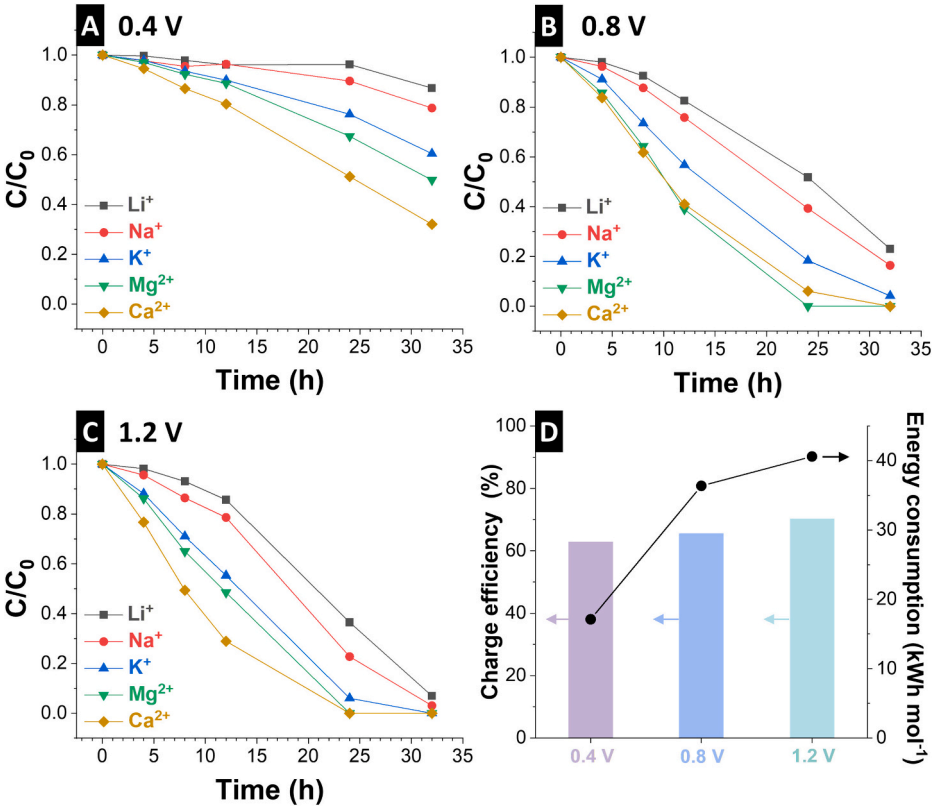

Fig. 7. Ion separation at (A) 0.4 V, (B) 0.8 V, and (C) 1.2 V applied potential at a flow rate of 6 mL min^{-1} for flow electrode and 2 mL min^{-1} for feed water, with 10 mass% of AC1 and 1 mass% CB. (D) Charge efficiency and energy consumption at different cell voltages.

would translate to around 0.19 € and almost half of that for non-household (such as industrial) consumers. In total, the material cost of 0.06 € and energy consumption of 0.19 € sum up to 0.25 € per cycle. The latter value is estimated for our laboratory-scale setup, assuming no energy recovery during discharging in a parallel system and that each carbon slurry is discarded after one charge. As the FCDI technology scales and matures, these costs could significantly decrease, making FCDI a more competitive and sustainable option for large-scale water treatment and resource recovery applications.

3.5. Effect of slurry and feed flow rate

In the last step to optimizing the FCDI system operation, we turned to the flow rate of electrode slurry and feed water to examine their potential impacts on the ion removal performance. Generally, a higher feed water flow rate promotes more ion accessibility toward the electrode surface in CDI, causing ions to be captured by electrode material to reach saturation more rapidly. [82] However, an excessively high flow rate could impede effective contact and interaction between ions and electrode surface, reducing adsorption capacity and desalination efficiency. [75] Hence, it is crucial to balance the cation separation efficiency and energy consumption (for pumping) when aiming for optimal ion removal through solution flow rate adjustments. As such, we investigated the flow rate as another influential parameter for our FCDI system by varying the slurry and feed flow rates and measuring the cation separation performance.

By keeping a constant feed flow rate of 2 mL min^{-1} and varying the slurry flow rate from 6 mL min^{-1} to 12 mL min^{-1} (Fig. 8A–B), no noticeable change was observed for the cation separation profiles of different ions. Further boosting the slurry flow rate to 24 mL min^{-1} also barely resulted in performance enhancements. As such, a slurry flow rate of 6 mL min^{-1} is chosen as an optimum value for further tests. The lower flow rate is also associated with lower pumping energy, minimizing the operational cost and energy consumption for potential scaling-up applications. The negligible effect of increased slurry flow rate on the cation separation could indicate that the ion migration and mobility on the slurry side are not rate-determining stages. Upon applying an electric field, the critical process and rate-controlling step will be the migration of charged ions from the feed's bulk solution side to the electrode channel through the cation exchange membrane. This is seen from the significant changes in ion separation profiles induced by varying feed flow rates (Fig. 8D–F).

By keeping the slurry flow rate constant at 6 mL min^{-1} and reducing the flow rate of feed water from 2 mL min^{-1} to 1 mL min^{-1}, the overall removal performance of ions, especially bivalent cations Ca^{2+} and Mg^{2+} decreased notably, which could be leveraged to adjust the ion selectivity performance of the FCDI system. For instance, at the operation time of 12 h, calculated selectivity factors of bivalent Ca^{2+} and Mg^{2+} ions versus Li^{+} were 1.4 and 1.9, respectively, for a feed rate of 1 mL min^{-1}. In contrast, the selectivity factors of Ca^{2+} and Mg^{2+} vs. Li^{+} were 5.8 and 4.7, respectively, at a feed rate of 2 mL min^{-1}. Increasing the feed water flow rate from 2 mL min^{-1} to 4 mL min^{-1} decreased the overall ion removal performance kinetics, corresponding to fewer ions transported from the feed channel to the slurry side due to the shorter retention time of feed water in the cell.

4. Conclusions

This study highlights FCDI for continuous cation separation from water. Our work evaluated a set of different activated carbon materials together with various contents of carbon additives as flowable electrodes. In addition, various operational parameters, including cell voltage and feed water flow rate and slurry, were investigated to optimize the FCDI ion sorption performance toward a multi-ion salt solution (Li^{+}, Na^{+}, K^{+}, Ca^{2+}, Mg^{2+}). The bivalent Ca^{2+} and Mg^{2+} ions were preferentially removed with faster kinetics due to their higher charge-to-size ratio, followed by K^{+}, Na^{+}, and Li^{+} in the order of their hydrated ion sizes. The optimum operational parameters for our FCDI system were identified: flow rate of electrode slurry at 6 mL min^{-1} and feed water at 2 mL min^{-1}, with 10 mass% activated carbon and 1 mass% carbon black at a cell voltage of 1.2 V. The system achieved average ion separation rates ranging from 5.7 μg cm^{-2} min^{-1} for Ca^{2+} to 0.2 μg cm^{-2} min^{-1} for

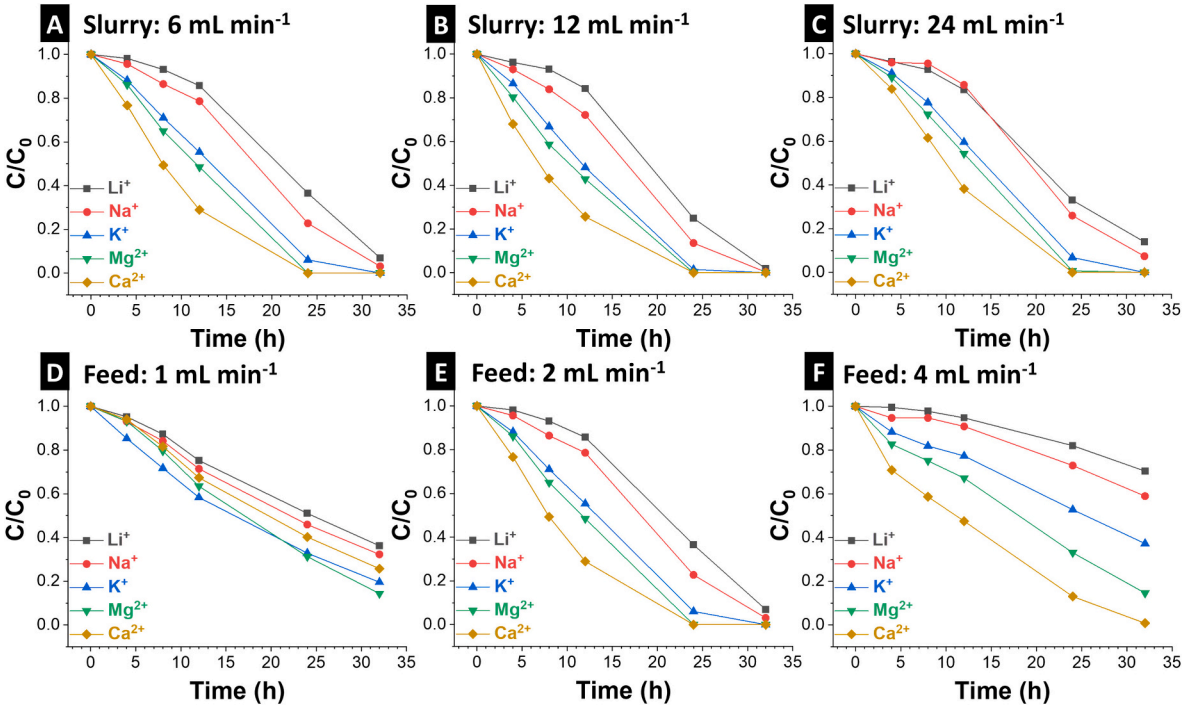

Fig. 8. Ion separation curves at varied slurry flow rates: (A) 6 mL min^{-1}, (B) 12 mL min^{-1}, and (C) 24 mL min^{-1}, with feed flow rate fixed at 2 mL min^{-1}; Ion separation curves at different flow rates of feed water: (D) 1 mL min^{-1}, (E) 2 mL min^{-1} and (F) 4 mL min^{-1}, with the flow rate of slurry fixed at 6 mL min^{-1}.

Li^+. An average energy consumption of ~41 Wh mol^{-1} was shown to be required to remove almost all the cations in the feed solution within 32 h of operation, which occurred at a cell voltage of 1.2 V with the highest charge efficiency of 70 %. We further showed how the adjustment of each operational parameter (except for slurry flow rate) could be leveraged to induce selectivity toward specific ions. In our experiments, we have seen the lowest uptake for lithium ions in competition with other monovalent cations or bivalent cations. This can be used to pre-treat, for example, hydrothermal water or hydrometallurgical battery recycling leaching solutions so that ions other than lithium ions are stripped to obtain an effluent stream with higher lithium ion contents. Overall, the findings contribute to the understanding and insights into FCDI technology and its potential application in sustainable water treatment and resource recovery efforts.

CRediT authorship contribution statement

Panyu Ren: Investigation, Data curation, Visualization, Writing – original draft, Writing – review & editing. **Bin Wang:** Investigation, Data curation, Visualization, Writing – original draft, Writing – review & editing. **Jean Gustavo de Andrade Ruthes:** Investigation, Data curation, Visualization, Writing – original draft, Writing – review & editing. **Mohammad Torkamanzadeh:** Investigation, Data curation, Visualization, Writing – original draft, Writing – review & editing. **Volker Presser:** Conceptualization, Supervision, Validation, Resources, Visualization, Writing – original draft, Writing – review & editing, Project administration, Funding acquisition.

Declaration of competing interest

The authors declare the following financial interests/personal relationships which may be considered as potential competing interests: Volker Presser reports financial support was provided by German Research Foundation. If there are other authors, they declare that they have no known competing financial interests or personal relationships that could have appeared to influence the work reported in this paper.

Data availability

Raw data are available upon request from the corresponding author.

Acknowledgments

We acknowledge funding of the SELECT project (PR 1173/33) by the German Research Foundation (DFG, Deutsche Forschungsgemeinschaft). B.W. acknowledges funding from the China Scholarship Council (CSC) via award number 202206270142.

Appendix A. Supplementary data

Supplementary data to this article can be found online at https://doi.org/10.1016/j.desal.2024.118161.

References

[1] M.A. Shannon, P.W. Bohn, M. Elimelech, J.G. Georgiadis, B.J. Mariñas, A. M. Mayes, Science and technology for water purification in the coming decades, Nature 452 (7185) (2008) 301–310.
[2] A.N. Shocron, R.S. Roth, E.N. Guyes, R. Epsztein, M.E. Suss, Comparison of ion selectivity in electrodialysis and capacitive deionization, Environ. Sci. Technol. Lett. 9 (11) (2022) 889–899.
[3] Z. Sahray, A.N. Shocron, R. Uwayid, C.E. Diesendruck, M.E. Suss, Extreme monovalent ion selectivity via capacitive ion exchange, Water Res. 246 (2023) 120684.
[4] S.-J. Seo, H. Jeon, J.K. Lee, G.-Y. Kim, D. Park, H. Nojima, J. Lee, S.-H. Moon, Investigation on removal of hardness ions by capacitive deionization (CDI) for water softening applications, Water Res. 44 (7) (2010) 2267–2275.
[5] H.H. Kyaw, M.T.Z. Myint, S. Al-Harthi, M. Al-Abri, Removal of heavy metal ions by capacitive deionization: effect of surface modification on ions adsorption, J. Hazard. Mater. 385 (2020) 121565.
[6] L. Xu, C. Yu, Y. Mao, Y. Zong, B. Zhang, H. Chu, D. Wu, Can flow-electrode capacitive deionization become a new in-situ soil remediation technology for heavy metal removal? J. Hazard. Mater. 402 (2021) 123568.
[7] R. Chen, T. Sheehan, J.L. Ng, M. Brucks, X. Su, Capacitive deionization and electrosorption for heavy metal removal, Environmental Science: Water Research & Technology 6 (2) (2020) 258–282.
[8] L. Wang, S. Arnold, P. Ren, Q. Wang, J. Jin, Z. Wen, V. Presser, Redox flow battery for continuous and energy-effective lithium recovery from aqueous solution, ACS Energy Lett. 7 (10) (2022) 3539–3544.
[9] A.A.M. Abusultan, J.A. Wood, T. Sainio, A.J.B. Kemperman, W.G.J. van der Meer, Ion exchange resin - bipolar membrane electrodialysis hybrid process for reverse osmosis permeate remineralization: preparative ion exchange chromatography for $C^{a2}{}_+$ and Mg^{2+} recovery, Sep. Purif. Technol. 317 (2023) 123799.
[10] M. Hafiz, R. Alfahel, A. Altaee, A.H. Hawari, Techno-economic assessment of forward osmosis as a pretreatment process for mitigation of scaling in multi-stage flash seawater desalination process, Sep. Purif. Technol. 309 (2023) 123007.
[11] S.B. Rauer, S. Wang, N. Köller, D.J. Bell, Y. Zhang, X. Wang, C.J. Linnartz, M. Wessling, J. Linkhorst, PEDOT:PSS-CNT composite particles overcome contact resistances in slurry electrodes for flow-electrode capacitive deionization, Adv. Funct. Mater. 33 (38) (2023) 2303606.
[12] L. Wang, Y. Zhang, K. Moh, V. Presser, From capacitive deionization to desalination batteries and desalination fuel cells, Curr. Opin. Electrochem. 29 (1) (2021) 100758.
[13] J.G. Gamaethiralalage, K. Singh, S. Sahin, J. Yoon, M. Elimelech, M.E. Suss, P. Liang, P.M. Biesheuvel, R.L. Zornitta, L.C.P.M. de Smet, Recent advances in ion selectivity with capacitive deionization, Energ. Environ. Sci. 14 (3) (2021) 1095–1120.
[14] J.W. Blair, G.W. Murphy, Electrochemical Demineralization of Water with Porous Electrodes of Large Surface Area, Saline Water Conversion, American Chemical Society1960, pp. 206–223.
[15] P. Ren, M. Torkamanzadeh, X. Zhang, M. Twardoch, C. Kim, V. Presser, Conductive carbon additives: friend or foe of capacitive deionization with activated carbon? Carbon 213 (2023) 118191.
[16] Y. Zhang, P. Ren, L. Wang, E. Pameté, S. Husmann, V. Presser, Selectivity toward heavier monovalent cations of carbon ultramicropores used for capacitive deionization, Desalination 542 (2022) 116053.
[17] Q. Dong, X. Guo, X. Huang, L. Liu, R. Tallon, B. Taylor, J. Chen, Selective removal of lead ions through capacitive deionization: role of ion-exchange membrane, Chem. Eng. J. 361 (2019) 1535–1542.
[18] Y. Sun, Y. Su, Z. Zhao, J. Zhao, M. Ye, X. Wen, Capacitive heavy metal ion removal of 3D self-supported nitrogen-doped carbon-encapsulated titanium nitride nanorods via the synergy of faradic-reaction and electro-adsorption, Chem. Eng. J. 443 (2022) 136542.
[19] T.K.A. Nguyen, N.T.N. Anh, M.D. Nguyen, V.T. Nguyen, R.-a. Doong, Boosting capacitive deionization of monovalent and hardness ions using Ti3C2Tx MXene as an intercalation-type pseudocapacitive electrode, Sep. Purif. Technol. 327 (2023) 124934.
[20] Y. Xu, S. Xiang, H. Zhou, G. Wang, H. Zhang, H. Zhao, Intrinsic pseudocapacitive affinity in manganese spinel ferrite nanospheres for high-performance selective capacitive removal of Ca^{2+} and Mg^{2+}, ACS Appl. Mater. Interfaces 13 (32) (2021) 38886–38896.
[21] W. Deng, Y. Chen, Z. Wang, X. Chen, M. Gao, F. Chen, W. Chen, T. Ao, Regulation, quantification and application of the effect of functional groups on anion selectivity in capacitive deionization, Water Res. 222 (2022) 118927.
[22] M.E. Suss, S. Porada, X. Sun, P.M. Biesheuvel, J. Yoon, V. Presser, Water desalination via capacitive deionization: what is it and what can we expect from it? Energ. Environ. Sci. 8 (8) (2015) 2296–2319.
[23] Y. Gendel, A.K.E. Rommerskirchen, O. David, M. Wessling, Batch mode and continuous desalination of water using flowing carbon deionization (FCDI) technology, Electrochem. Commun. 46(0) (2014) 152–156.
[24] S.I. Jeon, H.R. Park, J.G. Yeo, S. Yang, C.H. Cho, M.H. Han, D.K. Kim, Desalination via a new membrane capacitive deionization process utilizing flow-electrodes, Energ. Environ. Sci. 6 (5) (2013) 1471–1475.
[25] C. Kim, P. Srimuk, J. Lee, M. Aslan, V. Presser, Semi-continuous capacitive deionization using multi-channel flow stream and ion exchange membranes, Desalination 425 (2018) 104–110.
[26] L. Zhang, R. Feng, W. Wang, G. Yu, Emerging chemistries and molecular designs for flow batteries, Nat. Rev. Chem. 6 (8) (2022) 524–543.
[27] A. Rommerskirchen, Y. Gendel, M. Wessling, Single module flow-electrode capacitive deionization for continuous water desalination, Electrochem. Commun. 60 (2015) 34–37.
[28] A. Rommerskirchen, C.J. Linnartz, F. Egidi, S. Kendir, M. Wessling, Flow-electrode capacitive deionization enables continuous and energy-efficient brine concentration, Desalination 490 (2020) 114453.
[29] J. Ma, L. Chen, F. Yu, Environmental applications and perspectives of flow electrode capacitive deionization (FCDI), Sep. Purif. Technol. 335 (2024) 126095.
[30] J. Ma, C.X. Zhai, F. Yu, Review of flow electrode capacitive deionization technology: research progress and future challenges, Desalination 564 (2023) 116701.
[31] B. Xie, Q. Liu, C. Hu, H. Li, G. Tan, D. Xiao, Enhanced desalination performance in flow electrode capacitive deionization with nitrogen doped porous carbon, New J. Chem. 47 (18) (2023) 8625–8637.

[32] C. He, J. Ma, C. Zhang, J. Song, T.D. Waite, Short-circuited closed-cycle operation of flow-electrode CDI for brackish water softening, Environ. Sci. Technol. 52 (16) (2018) 9350–9360.
[33] N. Köller, M. Perrey, L.K. Brückner, P. Schäfer, S. Werner, C.J. Linnartz, M. Wessling, Comparison of current collector architectures for flow-electrode capacitive deionization, Desalination 582 (2024) 117595.
[34] J. Oladunni, J.H. Zain, A. Hai, F. Banat, G. Bharath, E. Alhseinat, A comprehensive review on recently developed carbon based nanocomposites for capacitive deionization: from theory to practice, Sep. Purif. Technol. 207 (2018) 291–320.
[35] P. Sivasubramanian, M. Kumar, V.S. Kirankumar, M.S. Samuel, C.D. Dong, J. H. Chang, Capacitive deionization and electrosorption techniques with different electrodes for wastewater treatment applications, Desalination 559 (2023) 116652.
[36] X. Zhang, K. Zuo, X. Zhang, C. Zhang, P. Liang, Selective ion separation by capacitive deionization (CDI) based technologies: a state-of-the-art review, Environmental Science: Water Research & Technology 6 (2) (2020) 243–257.
[37] E.N. Guyes, A.N. Shocron, Y. Chen, C.E. Diesendruck, M.E. Suss, Long-lasting, monovalent-selective capacitive deionization electrodes, npj clean, Water 4 (1) (2021) 22.
[38] M.E. Suss, Size-based ion selectivity of micropore electric double layers in capacitive deionization electrodes, J. Electrochem. Soc. 164 (9) (2017) E270.
[39] R. Uwayid, E.N. Guyes, A.N. Shocron, J. Gilron, M. Elimelech, M.E. Suss, Perfect divalent cation selectivity with capacitive deionization, Water Res. 210 (2022) 117959.
[40] P. Srimuk, X. Su, J. Yoon, D. Aurbach, V. Presser, Charge-transfer materials for electrochemical water desalination, ion separation and the recovery of elements, Nat. Rev. Mater. 5 (7) (2020) 517–538.
[41] Y. Xu, H. Zhou, G. Wang, Y. Zhang, H. Zhang, H. Zhao, Selective pseudocapacitive deionization of calcium ions in copper hexacyanoferrate, ACS Appl. Mater. Interfaces 12 (37) (2020) 41437–41445.
[42] K. Singh, G. Li, J. Lee, H. Zuilhof, B.L. Mehdi, R.L. Zornitta, L.C.P.M. de Smet, Divalent ion selectivity in capacitive deionization with vanadium hexacyanoferrate: experiments and quantum-chemical computations, Adv. Funct. Mater. 31 (41) (2021) 2105203.
[43] Y. Gao, L. Pan, H. Li, Y. Zhang, Z. Zhang, Y. Chen, Z. Sun, Electrosorption behavior of cations with carbon nanotubes and carbon nanofibres composite film electrodes, Thin Solid Films 517 (5) (2009) 1616–1619.
[44] X. Zhang, F. Yang, J. Ma, P. Liang, Effective removal and selective capture of copper from salty solution in flow electrode capacitive deionization, Environ. Sci.: Water Res. Technol. 6 (2) (2020) 341–350.
[45] L. Xu, C. Yu, S. Tian, Y. Mao, Y. Zong, X. Zhang, B. Zhang, C. Zhang, D. Wu, Selective recovery of phosphorus from synthetic urine using flow-electrode capacitive deionization (FCDI)-based technology, ACS ES&T Water 1 (1) (2021) 175–184.
[46] T.M. Khoi, N.A.T. Tran, H.B. Jung, V.P. Huynh, Y. Kim, J. Hong, C.-Y. Yoo, H. S. Kang, Y. Cho, Selective and continuous ion recovery using flow electrode capacitive deionization with polymer multilayers functionalized ion exchange membrane, Desalination 558 (2023) 116626.
[47] C. Zhang, J. Ma, L. Wu, J. Sun, L. Wang, T. Li, T.D. Waite, Flow electrode capacitive deionization (FCDI): recent developments, environmental applications, and future perspectives, Environ. Sci. Technol. 55 (8) (2021) 4243–4267.
[48] D. Moreno, M.C. Hatzell, Influence of feed-electrode concentration differences in flow-electrode Systems for Capacitive Deionization, Ind. Eng. Chem. Res. 57 (26) (2018) 8802–8809.
[49] S. Yang, J. Choi, J.-g. Yeo, S.-i. Jeon, H.-r. Park, D.K. Kim, Flow-electrode capacitive deionization using an aqueous electrolyte with a high salt concentration, Environ. Sci. Technol. 50(11) (2016) 5892–5899.
[50] M. Torkamanzadeh, C. Kök, P.R. Burger, P. Ren, Y. Zhang, J. Lee, C. Kim, V. Presser, Best practice for electrochemical water desalination data generation and analysis, Cell Reports Physical Science 4 (11) (2023) 101661.
[51] Z. Chen, H. Zhang, C. Wu, Y. Wang, W. Li, A study of electrosorption selectivity of anions by activated carbon electrodes in capacitive deionization, Desalination 369 (2015) 46–50.
[52] H. Li, L. Zou, L. Pan, Z. Sun, Using graphene nano-flakes as electrodes to remove ferric ions by capacitive deionization, Sep. Purif. Technol. 75 (1) (2010) 8–14.
[53] S.H. Lee, J.C. Rasaiah, Molecular dynamics simulation of ion mobility. 2. Alkali metal and halide ions using the SPC/E model for water at 25 °C, J. Phys. Chem. 100 (4) (1996) 1420–1425.
[54] S. Nadakatti, M. Tendulkar, M. Kadam, Use of mesoporous conductive carbon black to enhance performance of activated carbon electrodes in capacitive deionization technology, Desalination 268 (1) (2011) 182–188.
[55] A. Carmona-Orbezo, R.A.W. Dryfe, Understanding the performance of flow-electrodes for capacitive deionization through hydrodynamic voltammetry, Chem. Eng. J. 406 (2021) 126826.
[56] B. Akuzum, P. Singh, D.A. Eichfeld, L. Agartan, S. Uzun, Y. Gogotsi, E.C. Kumbur, Percolation characteristics of conductive additives for capacitive flowable (semi-solid) electrodes, ACS Appl. Mater. Interfaces 12 (5) (2020) 5866–5875.
[57] C.L. Barrie, P.C. Griffiths, R.J. Abbott, I. Grillo, E. Kudryashov, C. Smyth, Rheology of aqueous carbon black dispersions, J. Colloid Interface Sci. 272 (1) (2004) 210–217.
[58] Y. Wang, R.H. Ewoldt, New insights on carbon black suspension rheology - anisotropic thixotropy and antithixotropy, Journal of Rheology 66 (5) (2022) 937–953.
[59] M. Tauk, M. Bechelany, S. Lagerge, P. Sistat, R. Habchi, M. Cretin, F. Zaviska, Influence of particle size distribution on carbon-based flowable electrode viscosity and desalination efficiency in flow electrode capacitive deionization, Sep. Purif. Technol. 306 (2023) 122666.
[60] A. Narayanan, F. Mugele, M.H.G. Duits, Mechanical history dependence in carbon black suspensions for flow batteries: a rheo-impedance study, Langmuir 33 (7) (2017) 1629–1638.
[61] H. Hou, C.C. Sun, Quantifying effects of particulate properties on powder flow properties using a ring shear tester, J. Pharm. Sci. 97 (9) (2008) 4030–4039.
[62] G. Barthelmes, S.E. Pratsinis, H. Buggisch, Particle size distributions and viscosity of suspensions undergoing shear-induced coagulation and fragmentation, Chem. Eng. Sci. 58 (13) (2003) 2893–2902.
[63] J.B. Hipp, J.J. Richards, N.J. Wagner, Structure-property relationships of sheared carbon black suspensions determined by simultaneous rheological and neutron scattering measurements, J. Rheol. 63 (3) (2019) 423–436.
[64] G. Folaranmi, M. Tauk, M. Bechelany, P. Sistat, M. Cretin, F. Zaviska, Investigation of fine activated carbon as a viable flow electrode in capacitive deionization, Desalination 525 (2022) 115500.
[65] H.-r. Park, J. Choi, S. Yang, S.J. Kwak, S.-i. Jeon, M.H. Han, D.K. Kim, Surface-modified spherical activated carbon for high carbon loading and its desalting performance in flow-electrode capacitive deionization, RSC Adv. 6(74) (2016) 69720–69727.
[66] J. Lee, D. Weingarth, I. Grobelsek, V. Presser, Use of surfactants for continuous operation of aqueous electrochemical flow capacitors, Energ. Technol. 4 (1) (2016) 75–84.
[67] K.B. Hatzell, M.C. Hatzell, K.M. Cook, M. Boota, G.M. Housel, A. McBride, E. C. Kumbur, Y. Gogotsi, Effect of oxidation of carbon material on suspension electrodes for flow electrode capacitive deionization, Environ. Sci. Technol. 49 (5) (2015) 3040–3047.
[68] L. Firdaous, J.P. Malériat, J.P. Schlumpf, F. Quéméneur, Transfer of monovalent and divalent cations in salt solutions by Electrodialysis, Sep. Sci. Technol. 42 (5) (2007) 931–948.
[69] Y. Marcus, Ionic radii in aqueous solutions, Chem. Rev. 88 (8) (1988) 1475–1498.
[70] R.W. Impey, P.A. Madden, I.R. McDonald, Hydration and mobility of ions in solution, J. Phys. Chem. 87 (25) (1983) 5071–5083.
[71] J. Luo, S. Ye, T. Li, E. Sarnello, H. Li, T. Liu, Distinctive trend of metal binding affinity via hydration shell breakage in nanoconfined cavity, J. Phys. Chem. C 123 (23) (2019) 14825–14833.
[72] K. Tang, S. Yiacoumi, Y. Li, C. Tsouris, Enhanced water desalination by increasing the electroconductivity of carbon powders for high-performance flow-electrode capacitive deionization, ACS Sustainable Chemistry & Engineering 7 (1) (2019) 1085–1094.
[73] I. Hwang, D. Lee, Y. Jung, K. Park, Y.-G. Jung, D. Kim, G.-H. Cho, S.-i. Jeon, Y.-k. Byeun, U. Paik, S. Yang, T. Song, Cross effect of surface area and electrical conductivity for carbonaceous materials in flow-electrode capacitive mixing (F-CapMix) and flow-electrode capacitive deionization (FCDI): solid-like behavior of flow-electrode, ACS Sustain. Chem. Eng. 9(40) (2021) 13514–13525.
[74] E.R. Reale, A. Shrivastava, K.C. Smith, Effect of conductive additives on the transport properties of porous flow-through electrodes with insulative particles and their optimization for faradaic deionization, Water Res. 165 (2019) 114995.
[75] S. Chai, J. Xi, L. Chen, W. He, J. Shen, H. Gong, Selective ion removal by capacitive deionization (CDI)-based technologies, Processes 10 (6) (2022) 1075.
[76] M. Torkamanzadeh, L. Wang, Y. Zhang, Ö. Budak, P. Srimuk, V. Presser, MXene/activated-carbon hybrid capacitive deionization for permselective ion removal at low and high salinity, ACS Appl. Mater. Interfaces 12 (23) (2020) 26013–26025.
[77] S. Porada, D. Weingarth, H.V.M. Hamelers, M. Bryjak, V. Presser, P.M. Biesheuvel, Carbon flow electrodes for continuous operation of capacitive deionization and capacitive mixing energy generation, J. Mater. Chem. A 2 (24) (2014) 9313–9321.
[78] Y.-U. Shin, J. Lim, C. Boo, S. Hong, Improving the feasibility and applicability of flow-electrode capacitive deionization (FCDI): review of process optimization and energy efficiency, Desalination 502 (2021) 114930.
[79] E. Guillén-Burrieza, D.-C. Alarcón-Padilla, P. Palenzuela, G. Zaragoza, Techno-economic assessment of a pilot-scale plant for solar desalination based on existing plate and frame MD technology, Desalination 374 (2015) 70–80.
[80] N. Köller, L. Mankertz, S. Finger, C.J. Linnartz, M. Wessling, Towards pilot scale flow-electrode capacitive deionization, Desalination 572 (2024) 117096.
[81] R. Kayiwa, H. Kasedde, M. Lubwama, J.B. Kirabira, The potential for commercial scale production and application of activated carbon from cassava peels in Africa: a review, Bioresource Technology Reports 15 (2021) 100772.
[82] Y. Zhang, P. Ren, Y. Liu, V. Presser, Particle size distribution influence on capacitive deionization: insights for electrode preparation, Desalination 525 (2022) 115503.